RESEARCH ARTICLE SUMMARY

IMMUNOGENETICS

Dynamic profiling of the protein life cycle in response to pathogens

Marko Jovanovic,* Michael S. Rooney,* Philipp Mertins, Dariusz Przybylski, Nicolas Chevrier, Rahul Satija, Edwin H. Rodriguez, Alexander P. Fields, Schraga Schwartz, Raktima Raychowdhury, Maxwell R. Mumbach, Thomas Eisenhaure, Michal Rabani, Dave Gennert, Diana Lu, Toni Delorey, Jonathan S. Weissman, Steven A. Carr, Nir Hacohen,† Aviv Regev†

INTRODUCTION: Mammalian gene expression is tightly controlled through the interplay between the RNA and protein life cycles. Although studies of individual genes have shown that regulation of each of these processes is important for correct protein expression, the quantitative contribution of each step to changes in protein expression levels remains largely unknown and much debated. Many studies have attempted to address this question in the context of steady-state protein levels, and comparing steady-state RNA and protein abundances has indicated a considerable discrepancy between RNA and protein levels. In contrast, only a few studies have attempted to shed light on how changes in each of these processes determine differential protein expression—either relative (ratios) or absolute (differences)—during dynamic responses, and only one recent report has attempted to quantitate each process. Understanding these contributions to a dynamic response on a systems scale is essential both for deciphering how cells deploy regulatory processes to accomplish physiological changes and for discovering key molecular regulators controlling each process.

RATIONALE: We developed an integrated experimental and computational strategy to quantitatively assess how protein levels are maintained in the context of a dynamic response and applied it to the model response of mouse immune bone marrow–derived dendritic cells (DCs) to stimulation with lipopolysaccharide (LPS). We used a modified pulsed-SILAC (stable isotope labeling with amino acids in cell culture) approach to track newly synthesized and previously labeled proteins over the first 12 hours of the response. In addition, we independently measured replicate RNA-sequencing profiles under the same conditions. We devised a computational strategy to infer per-mRNA translation rates and protein degradation rates at each time point from the temporal transcriptional profiles and pulsed-SILAC proteomics data. This allowed us to build a genome-scale quantitative model of the temporal dynamics of differential protein expression in DCs responding to LPS.

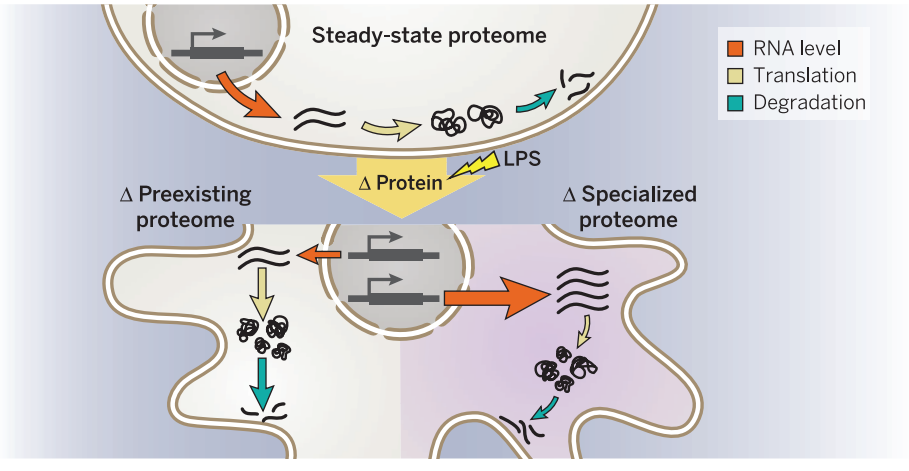

Dynamic protein expression regulation in dendritic cells upon stimulation with LPS. We developed an integrated experimental and computational strategy to quantitatively assess how protein levels are maintained in the context of a dynamic response. Our results support a model in which the induction of novel cellular functions is primarily driven through transcriptional changes, whereas regulation of protein production or degradation updates the levels of preexisting functions.

RESULTS: We found that before stimulation, mRNA levels contribute to overall protein expression levels more than double the combined contribution of protein translation and degradation rates. Upon LPS stimulation, changes in mRNA abundance play an even more dominant role in dynamic changes in protein levels, especially in immune response genes. Nevertheless, several protein modules—especially the preexisting proteome of proteins performing basic cellular functions—are predominantly regulated in stimulated cells at the level of protein translation or degradation, accounting for over half of the absolute change in protein molecules in the cell. In particular, despite the repression of their transcripts, the level of many proteins in the translational machinery is up-regulated upon LPS stimulation because of significantly increased translation rates, and elevated protein degradation of mitochondrial proteins plays a central role in remodeling cellular energy metabolism.

ON OUR WEB SITE

Read the full article at http://dx.doi.org/10.1126/science.1259038

CONCLUSIONS: Our results support a model in which the induction of novel cellular functions is primarily driven through transcriptional changes, whereas regulation of protein production or degradation updates the levels of preexisting functions as required for an activated state. Our approach for building quantitative genome-scale models of the temporal dynamics of protein expression is broadly applicable to other dynamic systems. ■

RELATED ITEMS IN *SCIENCE*

A. Battle *et al.*, *Science* **347**, 664 (2015)
DOI: 10.1126/science.1260793

The list of author affiliations is available in the full article online.
*These authors contributed equally to the work.
†Corresponding author. E-mail: aregev@broad.mit.edu (A.R.); nhacohen@mgh.harvard.edu (N.H.)
Cite this article as M. Jovanovic *et al.*, *Science* **347**, 1259038 (2015). DOI: 10.1126/science.1259038

RESEARCH ARTICLE

IMMUNOGENETICS

Dynamic profiling of the protein life cycle in response to pathogens

Marko Jovanovic,[1]* Michael S. Rooney,[1,2]* Philipp Mertins,[1] Dariusz Przybylski,[1] Nicolas Chevrier,[1,3] Rahul Satija,[1]†‡ Edwin H. Rodriguez,[4] Alexander P. Fields,[4] Schraga Schwartz,[1] Raktima Raychowdhury,[1] Maxwell R. Mumbach,[1] Thomas Eisenhaure,[1,5] Michal Rabani,[1]§ Dave Gennert,[1] Diana Lu,[1] Toni Delorey,[1] Jonathan S. Weissman,[4,6] Steven A. Carr,[1] Nir Hacohen,[1,5,7]† Aviv Regev[1,8,9]||

Protein expression is regulated by the production and degradation of messenger RNAs (mRNAs) and proteins, but their specific relationships remain unknown. We combine measurements of protein production and degradation and mRNA dynamics so as to build a quantitative genomic model of the differential regulation of gene expression in lipopolysaccharide-stimulated mouse dendritic cells. Changes in mRNA abundance play a dominant role in determining most dynamic fold changes in protein levels. Conversely, the preexisting proteome of proteins performing basic cellular functions is remodeled primarily through changes in protein production or degradation, accounting for more than half of the absolute change in protein molecules in the cell. Thus, the proteome is regulated by transcriptional induction for newly activated cellular functions and by protein life-cycle changes for remodeling of preexisting functions.

Mammalian gene expression is tightly controlled through the interplay between the RNA and protein life cycles (Fig. 1A). Although studies of individual genes have shown the importance of regulating each of these processes for correct protein expression (*1*–*4*), the quantitative contribution of each process to changes in protein expression levels (Fig. 1A) remains largely unknown and much debated (*5*, *6*). Many studies have attempted to address this question in the context of steady-state protein levels (*5*, *7*–*13*), and comparing steady-state mRNA and protein abundances has indicated a considerable discrepancy between mRNA and protein levels (*5*, *7*–*13*). Furthermore, protein expression is more conserved across species than is mRNA expression (*11*, *14*, *15*), both suggesting a substantial contribution of the protein life cycle. A recent study using metabolic pulse labeling of proteins and mRNA in an asynchronously proliferating mammalian cell line (*16*) concluded that gene-to-gene differences in protein synthesis rates contributed most to final protein levels (~55%), followed by mRNA abundance (40%), whereas degradation of mRNA and protein played only minor roles. However, reanalysis of this data challenged some of these conclusions, arguing that the contribution of mRNA levels could be as high as 84% and that of protein synthesis as low as 8% (*6*).

In contrast, only a few studies (*5*, *12*, *17*–*20*) have attempted to shed light on how changes in each of these processes determine differential protein expression—either relative (ratios) or absolute (differences)—during dynamic responses, and only one recent report (*20*) has attempted to quantitate each process. However, none of these has comprehensively accounted for experimental measurement errors, nor have they deconvolved interdependencies of the data. Understanding these contributions to a dynamic response on a systems scale is essential both for deciphering how cells deploy regulatory processes to accomplish physiological changes and for discovering key molecular regulators controlling each process.

Results

A pulsed-SILAC strategy to measure protein dynamics

We assessed how protein levels are maintained in the context of the model response of mouse immune bone marrow–derived dendritic cells (DCs) (*21*) to stimulation with lipopolysaccharide (LPS) (*22*–*26*). This is a compelling system because DCs are mostly postmitotic, and LPS synchronizes them (*27*) and causes dramatic regulatory changes from the expression of thousands of transcripts (*22*, *24*, *25*) to protein phosphorylation (*26*). To monitor protein production and degradation during a dynamic response, we used a modified pulsed-SILAC (stable isotope labeling with amino acids in cell culture) approach (Fig. 1B) (*28*, *29*) to track newly synthesized and previously labeled proteins over time. We cultured DCs for 9 days in medium-heavy–labeled (M) SILAC medium then substituted the M SILAC medium with heavy-labeled (H) SILAC medium and immediately stimulated them with LPS or medium (MOCK). Newly synthesized proteins were thus labeled with heavy (H) amino acids, serving as a proxy for protein synthesis, whereas proteins with medium-heavy (M) amino acids decayed over time, reflecting cellular half lives. For normalization, we spiked in a reference sample, extracted from a mix of unstimulated and stimulated DCs grown in light (L) SILAC media. We collected biological replicate samples at 10 time points over 12 hours (0, 0.5, 1, 2, 3, 4, 5, 6, 9, and 12 hours) after LPS or mock stimulation. We quantified 6079 proteins by means of liquid chromatography–tandem mass spectrometry (LC-MS/MS) in at least one sample and 2288 proteins in all samples (time points, conditions, and replicates) (Fig. 2A and table S1). We independently measured replicate RNA-sequencing (RNA-Seq) profiles under the same conditions (Fig. 2A and table S2) (*29*).

A model-based estimation of protein synthesis and degradation rates

We devised a computational strategy to infer per-mRNA translation rates [$T(t)$] and protein degradation rates [$D(t)$] at each time point from the temporal transcriptional profiles [$R(t)$] and H/L and M/L protein ratios [$H(t)$ and $M(t)$, respectively] (Fig. 1B and fig. S1) (*29*). We defined a model that describes the relevant processes and associated rates (such as translation rate and protein degradation rate) and then fitted the parameters (such as rates) in the model with our mRNA and protein data. Specifically, we used an ordinary differential equations model describing, for each gene i, the changes in $M_i(t)$ and $Hi(t)$ [$dM_i(t)/dt$ and $dH_i(t)/dt$, respectively] as a function of (i) a production term, governed by mRNA abundance $R_i(t)$ and a per-mRNA molecule translation rate constant, $T_i(t)$; and (ii) a degradation term, modeled as an exponential decay function, governed by a protein degradation rate constant, $D_i(t)$. Both terms are also affected by $\gamma(t)$, the global M SILAC label recycling rate (figs. S1 and S2) (*29*). All rate constants are dynamic, and the mRNA levels, per-mRNA translation rate constant, and protein degradation rate constant are also gene-specific. We modeled the change over time in the per-mRNA translation rate constant [$T_i(t)$] and in the degradation rate constant ([$D_i(t)$] as linear functions. This assumption reduces the number of free parameters, thus providing robustness while retaining the capacity to detect the effect of sustained changes, even if these changes do not manifest linearly in vivo (as in the case of step functions).

[1]The Broad Institute of MIT and Harvard, Cambridge, MA 02142, USA. [2]Division of Health Sciences and Technology, Massachusetts Institute of Technology, Cambridge, MA 02139, USA. [3]Harvard Faculty of Arts and Sciences Center for Systems Biology, Harvard University, Cambridge, MA 02138, USA. [4]Department of Cellular and Molecular Pharmacology, California Institute for Quantitative Biomedical Research, University of California, San Francisco, San Francisco, CA 94158, USA. [5]Center for Immunology and Inflammatory Diseases, Massachusetts General Hospital, Boston, MA 02114, USA. [6]Howard Hughes Medical Institute (HHMI), University of California, San Francisco, San Francisco, CA 94158, USA. [7]Harvard Medical School, Boston, MA 02115, USA. [8]Department of Biology, Massachusetts Institute of Technology, Cambridge, MA 02140, USA. [9]HHMI, Department of Biology, Massachusetts Institute of Technology, Cambridge, MA 02140, USA.
*These authors contributed equally to the work. †Present address: New York Genome Center, New York, NY 10013, USA. ‡Present address: Center for Genomics and Systems Biology, New York University, New York, NY 10012, USA. §Present address: Department of Molecular and Cellular Biology, Harvard University, Cambridge, MA 02138, USA. ||Corresponding author. E-mail: aregev@broad.mit.edu (A.R.); nhacohen@mgh.harvard.edu (N.H.)

We fitted the different parameters in the model (fig. S1) with the RNA-Seq and MS data (*29*) using an empirical Bayes strategy (*29*), which prevents overfitting of noisy MS data by sharing information across genes. In this approach, our most differential and reliable parameter estimates correspond to the well-quantified genes (*29*), whereas proteins with less reliable measurements are not associated with reliable changes. This ensures a low rate of false positives (calling a change where none exists) but may result in false negatives and, hence, in some underestimation of the contribution of protein synthesis and degradation.

Fitting the parameters for 3147 genes that passed our filtering criteria (*29*), separately for each of our replicates (Fig. 2B, fig. S3, and table S3), we found good reproducibility of the LPS/MOCK ratios of key fitted values (Fig. 2B and fig. S4) and of the relative differences in per-mRNA translation rates [for example, $\Delta T_i(12h) = T_i(12h)_{LPS}/T_i(12h)_{MOCK}$, Pearson correlation coefficient (r) = 0.68] (fig. S5A) or degradation rates [for example, $\Delta D_i(12h) = D_i(12h)_{LPS}/D_i(12h)_{MOCK}$, r = 0.62] (fig. S5B). The robustness of these results was further supported by (i) the fair correlation of our translation and protein degradation rate estimates in resting cells (table S3 and fig. S6, A and B) with previous estimates in mouse fibroblasts (NIH3T3) based on a similar pulsed-SILAC approach {$r[T_i(0)] = 0.35$; $r[D_i(0)] = 0.58$} (fig. S7) (*16*) or on estimates of translation rate efficiency (TE) values based on ribosome profiling in mouse fibroblasts (NIH3T3) {$r[T_i(0)] = 0.37$} (fig. S7C) (*30*); (ii) a good correlation between our per-mRNA translation rates and our independent measurement of TE values in DCs using ribosome profiling at time (t) = 0 hours (r = 0.5) (table S4) (fig. S8A), which is comparable with the correlation between TE values in mouse DCs and mouse fibroblasts (r = 0.54) (fig. S8B); (iii) that strong early changes are all in immune response proteins (fig. S4A); (iv) the global increase upon LPS stimulation in protein production rates [$T_i(12h)_{LPS}$ versus $T_i(12h)_{MOCK}$; $P < 10^{-10}$, Wilcoxon rank sum test] (fig. S9A) and protein degradation rates [$D_i(12h)_{LPS}$ versus $D_i(12h)_{MOCK}$; $P < 10^{-10}$, Wilcoxon rank sum test] (fig. S9B), which is consistent with other reports (*31*, *32*); and (v) the increase in the calculated "degradation rate"—likely reflecting depletion by secretion, or "decreased cellular half-life"—of proteins from the recently characterized secretome of LPS-stimulated mouse macrophages [$\delta D_i(12h) = D_i(12h)_{LPS}/D_i(12h)_{MOCK}$; $P < 10^{-10}$, Wilcoxon rank sum test] (fig. S9C) (*33*).

mRNA levels contribute the most to protein expression levels before stimulation

To determine the relative contribution of each step to steady-state protein levels in unstimulated, postmitotic DCs, we first estimated absolute protein levels from four additional MS data sets in resting DCs (0 hours) that rely on distinct peptides (*29*): two biological replicate samples, which were each digested in two technical replicates with LysN and AspN, respectively, rather than by trypsin, which was used for the pulsed SILAC samples (*29*).

Next, we assessed the contribution of each regulatory step to gene-to-gene differences in overall protein levels by comparing (with Spearman-corrected coefficients of determination) (*29*) the independently measured absolute protein levels to steady-state protein levels predicted by our model when setting one or more of the three regulatory steps (mRNA level, per-mRNA translation rate constant, or protein degradation rate constant) to its per-gene inferred value (at time 0 hours) and setting the remaining steps to their pan-genome median value (*29*). By sequentially adding to the model further per-gene values rather than pan-genome medians (such as mRNA level, translation rate, and last, degradation rate) and assessing the corresponding change in the correlation measure, we can assign additive regulatory contributions to the three steps (*29*). Because these three steps are not statistically independent from each other and may interact in a nonlinear manner, we explored every possible ordering of consideration.

Considering all three variables together, we account for nearly 79% of the variance of the independently measured protein levels (figs. S10 and S11A) (*29*). Of these 79%, mRNA levels explained 59 to 68%, per-mRNA translation rates 18 to 26%, and protein degradation rates 8 to 22% (Fig. 3A and fig. S11A) (*29*). We believe the unexplained variance is due to systematic errors in the measurements and modeling that could not be accounted for. In addition, we have separately estimated the variance in translation rates in the same cells under identical conditions using ribosome profiling to measure TE values [above and (*29*)]. Using

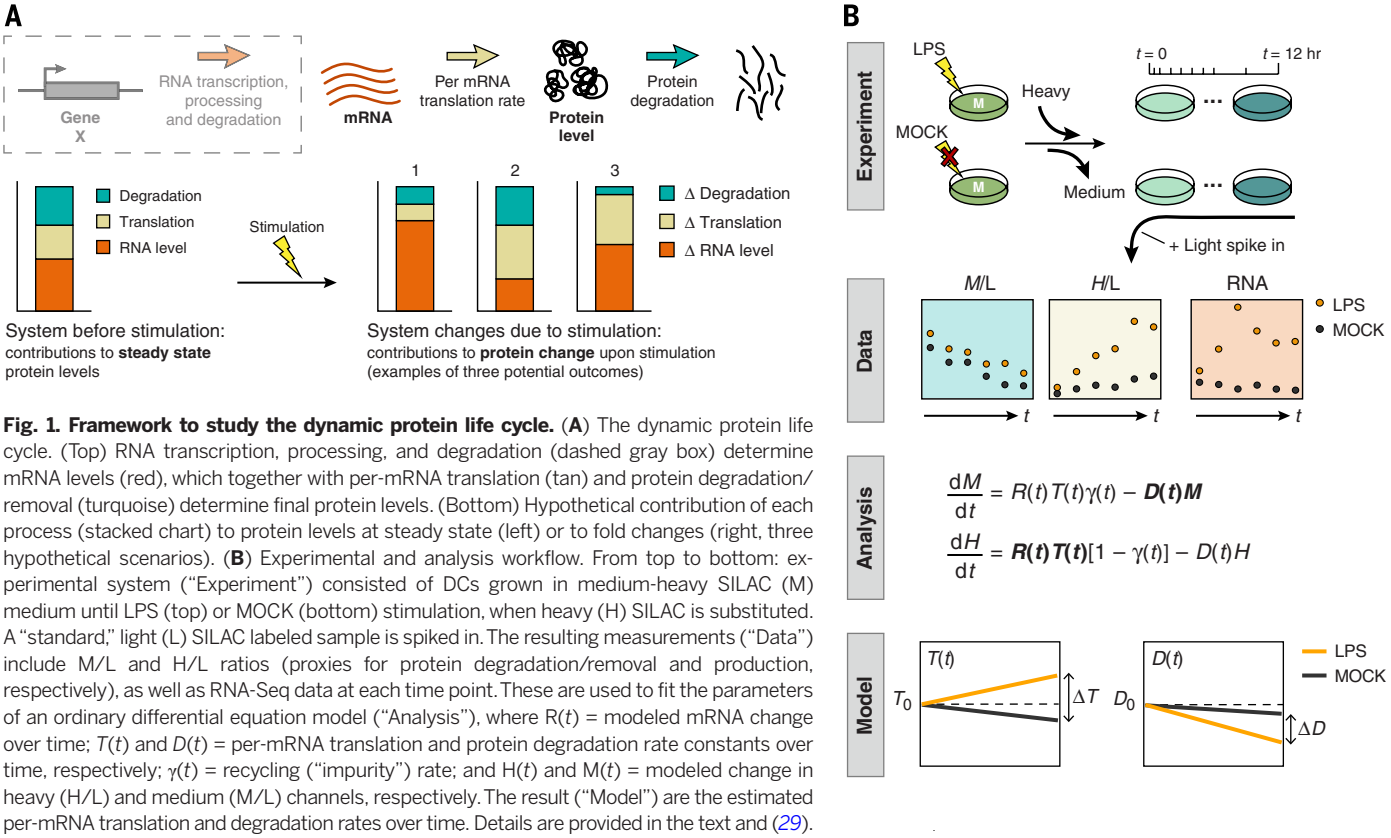

Fig. 1. Framework to study the dynamic protein life cycle. (**A**) The dynamic protein life cycle. (Top) RNA transcription, processing, and degradation (dashed gray box) determine mRNA levels (red), which together with per-mRNA translation (tan) and protein degradation/removal (turquoise) determine final protein levels. (Bottom) Hypothetical contribution of each process (stacked chart) to protein levels at steady state (left) or to fold changes (right, three hypothetical scenarios). (**B**) Experimental and analysis workflow. From top to bottom: experimental system ("Experiment") consisted of DCs grown in medium-heavy SILAC (M) medium until LPS (top) or MOCK (bottom) stimulation, when heavy (H) SILAC is substituted. A "standard," light (L) SILAC labeled sample is spiked in. The resulting measurements ("Data") include M/L and H/L ratios (proxies for protein degradation/removal and production, respectively), as well as RNA-Seq data at each time point. These are used to fit the parameters of an ordinary differential equation model ("Analysis"), where R(t) = modeled mRNA change over time; $T(t)$ and $D(t)$ = per-mRNA translation and protein degradation rate constants over time, respectively; $\gamma(t)$ = recycling ("impurity") rate; and H(t) and M(t) = modeled change in heavy (H/L) and medium (M/L) channels, respectively. The result ("Model") are the estimated per-mRNA translation and degradation rates over time. Details are provided in the text and (*29*).

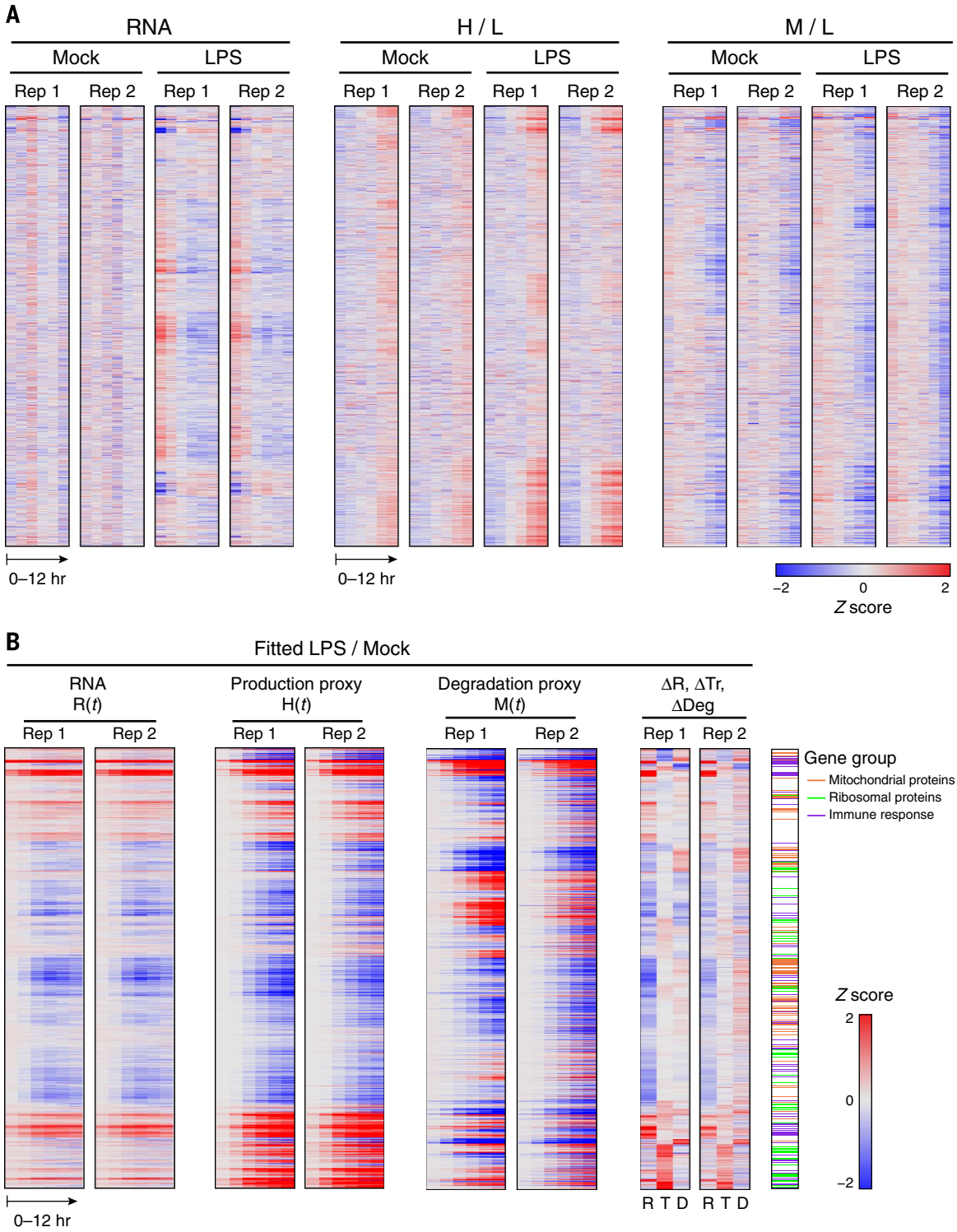

Fig. 2. The protein life cycle in LPS-stimulated DCs. (**A**) Shown are (left to right), for all 2288 genes (rows) that were quantified in all samples, mRNA expression, H/L protein expression, and M/L protein expression in LPS- and MOCK-stimulated DCs from each replicate (columns). Gene order is the same across all heatmaps and determined by means of hierarchical clustering of fitted fold changes in mRNA level, translation rate, and degradation rate. Values are median normalized by row, logged, and robust *z*-transformed per map (color scale). (**B**) Fitted differential expression of the same 2288 genes (rows). Left to right: Robust *z*-score fitted differential expression ratios (LPS/MOCK; red/blue color scale) for R(*t*), H(*t*), and M(*t*) in LPS- versus MOCK-stimulated DCs from each replicate (columns), with the $\log_2$ fold changes between LPS- and MOCK-stimulated DCs at 12 hours after stimulation for mRNA (ΔR), per-mRNA translation rate (ΔTr), and protein degradation rate (ΔDeg) (also *z*-scored). Rightmost column, immune response (purple), ribosomal (green), and mitochondrial (orange) proteins.

TE values instead of our pulsed-SILAC derived translation rates, we estimate a comparable contribution of protein synthesis (Fig. 3B and fig. S10). Thus, in postmitotic DCs, mRNA levels are contributing more to protein-to-protein variation in total protein levels than is the protein life cycle (synthesis and degradation rates combined).

mRNA abundance dynamics dominate protein changes after stimulation

Next, we determined the contribution of each regulatory step to protein fold changes at 12 hours. We used the model fit from a given replicate to predict the protein fold change at 12 hours, when using either MOCK-estimated parameters or one or more LPS-estimated parameters for mRNA level, translation rate, and degradation rate. We then compared these predictions to the fitted fold changes from the other replicate. Starting with all parameters set to MOCK-estimated rates, we sequentially used LPS-estimated parameters for mRNA, translation rate, and degradation rate (in every possible order) and thus assessed the contribution of each step as the increase in the Spearman-corrected coefficients of determination (*29*).

We found that mRNA levels explain ~87 to 92%, per-mRNA translation rates ~4 to 7%, and protein degradation rates ~3 to 6% of protein fold changes after 12 hours (Fig. 3C and fig. S11B) (*29*). mRNA fold changes contributed at least eight times as much as did the protein life cycle combined for both induced and repressed proteins (fig. S12 and table S5) (*29*). However, changes in per-mRNA translation rates contributed more substantially to protein-level induction, whereas changes in protein degradation rates mostly contributed to protein-level repression (fig. S12 and table S5) (*29*).

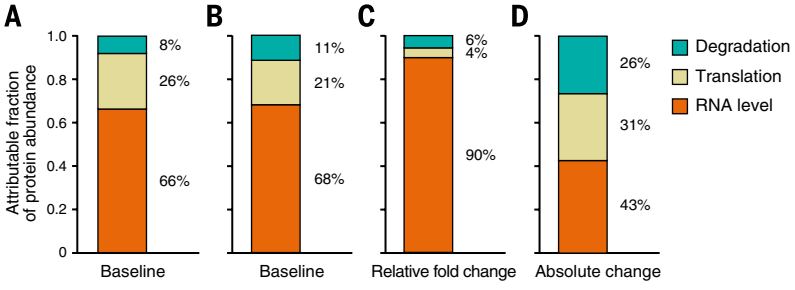

E

GSEA enrichments by regulatory mode (signed $\log_{10}$ *p*-values)

	Baseline RNA	Baseline translation	Baseline degradation	RNA fold change	Translation fold change	Degradation fold change
Endoplasmic reticulum lumen	0.5	0.8	1.6	1.4	−2.0	**8.7**
Lysosome	**5.0**	1.6	**−5.5**	1.7	**−10.9**	**13.2**
Extracellular region	**6.7**	4.0	0.4	**4.9**	−2.3	**8.4**
Mitochondrion	0.1	1.4	**−36.9**	**−11.5**	**−7.7**	**28.9**
Oxidation-reduction process	0.1	3.1	**−13.3**	**−9.1**	−4.3	**14.2**
Tricarboxylic acid cycle	1.1	3.1	**−6.9**	−3.1	**−4.8**	**8.0**
Metabolic process	**−7.0**	**4.8**	**−17.0**	**−4.6**	**−8.3**	**7.2**
Structural constituent of ribosome	**22.8**	**−7.8**	**−20.6**	−2.7	**12.6**	−0.5
Translation	**16.1**	−2.1	**−17.6**	−3.6	**10.8**	−3.0
Poly(A) RNA binding	**16.4**	−1.0	−3.0	−1.5	**10.8**	0.4
Actin binding	**5.0**	2.0	−2.7	0.3	4.3	**−5.8**
Respiratory chain	**8.5**	−3.2	−1.0	**−4.6**	−1.1	**6.3**
rRNA processing	1.2	−2.3	0.1	**−4.9**	3.3	0.2
Endonuclease activity	−0.5	0.0	1.4	**−4.5**	−0.3	1.5
Protein binding	3.6	1.2	**7.3**	**9.7**	**5.7**	**−6.6**
GTPase activator activity	−1.8	−0.7	0.5	−0.1	−1.2	**−6.3**
Cytoskeleton	1.4	0.1	1.3	0.1	2.9	**−12.8**
Cell projection	1.2	1.8	0.2	2.8	2.8	**−8.7**
Microtubule	−0.2	0.1	−0.1	0.4	1.5	**−6.3**
Protein kinase binding	1.4	1.5	0.1	2.8	**5.3**	**−5.1**
Immune response	1.1	0.5	**4.5**	**5.3**	−0.3	1.1
Cellular response to interferon-beta	**−4.4**	2.9	−0.4	**6.6**	0.2	−1.1
Defense response to virus	−3.3	−0.1	1.6	**7.3**	0.3	−0.3
Innate immune response	−0.4	1.3	2.6	**5.1**	0.9	0.1
Double-stranded RNA binding	−0.1	1.1	−0.6	**5.1**	2.5	−0.2

−15 0 15

Signed $\log_{10}$ *p*-value

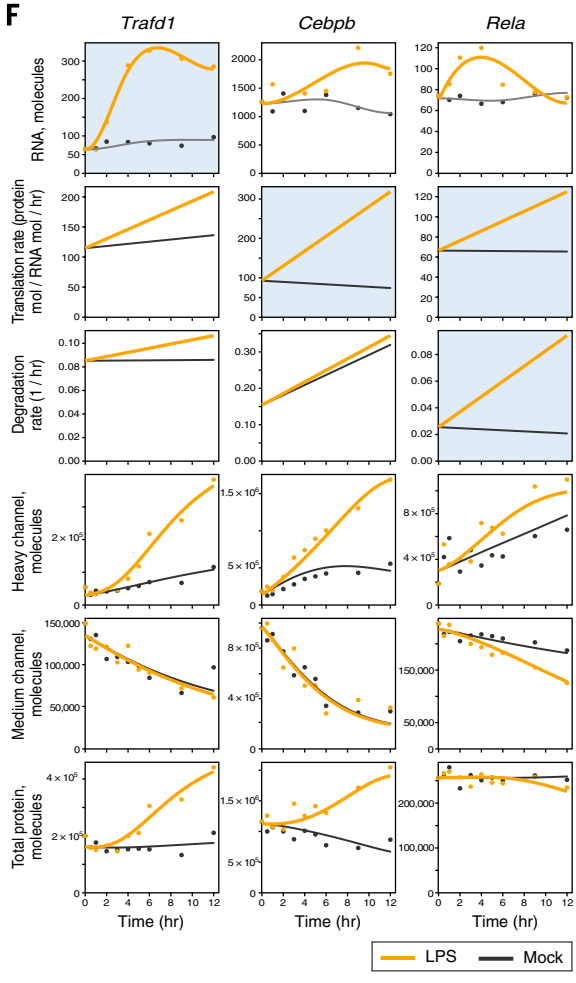

Fig. 3. Contributions of mRNA levels and the protein life cycle to steady-state and dynamic protein levels. (**A** to **D**) Global contributions of mRNA levels (orange), translation rates (tan), and protein degradation rates (turquoise) to protein levels. Translation rates were derived either from pulsed SILAC data [(A), (C), and (D)] or from TE values from ribosome profiling data (B). Contributions to steady-state protein levels before LPS induction [(A) and (B)] or to the change in protein abundance between LPS-induced and mock-treated cells [(C) and (D)] are shown. The contributions to the fold change (C) and to the absolute change in protein abundances (D) after LPS stimulation are given. The contributions for steady state presented exclude the percent of the variance in measured protein levels that is not explained by the variance in mRNA, translation, or protein degradation (fig. S10). Per-gene parameter values were in the order 1, mRNA; 2, translation; 3, degradation (*29*). All possible orderings are provided in fig. S11. (**E**) Functional processes controlled by distinct regulatory steps. For each process (rows) and regulatory step (columns) shown are the magnitudes of the $\log_{10}$(*P* values) for the values or differential fold changes (LPS/MOCK at 12 hours) of mRNA levels, protein synthesis, or degradation rates of genes annotated to this process versus the background of all genes fit by the model. Values are signed according to directionality of the enrichment (Wilcoxon rank sum test). Shown are the five gene sets most enriched for increased or decreased rates for the three "fold change" columns, along with their scores in all six regulatory modes. Nearly redundant gene sets were removed (all gene sets are available in table S6). (**F**) Examples of regulation of expression dynamics. For each of three genes in each of LPS (orange) and MOCK (black) condition shown are the measured values (dots) and fits (curves) for (top to bottom) mRNA levels (in mRNA molecules), per-mRNA translation rates (protein molecules/mRNA molecule/hour), degradation rates (1 per hour), H(t), M(t), and total protein [(M+H)(t)]; x axis, time; y axis, intensity or rate. Light blue indicates key regulatory mode. mRNA and protein molecules are only proxies for transcripts per million (TPM) and intensity-based absolute quantification (IBAQ) microshares, respectively, in order to help interpretation (*29*).

Fold changes in induced immune response proteins (29) were particularly dominated by mRNA level changes (Figs. 2B and 3E and table S6). For example, transient up-regulation of the mRNA encoding the negative immune regulator Trafd1 (Fig. 3F) (34) is the main cause of a strong increase in its protein. In Trafd1 and hundreds of other genes, a transient, strong, spiked change in mRNA, combined with a time-constant protein half-life much longer than the 12-hour time course, result in a monotonous increase in protein levels, so that global protein fold changes at 12 hours after LPS correlate best to mRNA changes at 5 hours (fig. S13). Only a handful of proteins [for example, Tnfaip2 (26, 35, 36)] show peaked, transient protein expression within our time scale; all have very high basal degradation rates, which typically do not increase further. Last, a few key regulators of DCs and the LPS response [such as CCAAT/enhancer-binding protein β (Cebpb), a pioneer transcription factor whose mRNA is already very highly expressed prestimulation, and Rela] (Fig. 3F) are considerably dynamically regulated at the protein level, so that increased protein degradation rates (Rela) and/or increased per-mRNA translation rates (Rela and Cebpb) are main drivers for protein change. These changes cannot be observed solely from total protein and transcript levels, but the corresponding rate changes are readily apparent (Fig. 3F).

Although our global model incorporates the data of only 3147 genes, several lines of evidence suggest that this did not bias our global conclusions. First, although the 3147 modeled genes are somewhat enriched for higher expressed genes (fig. S14), we do model a substantial number of lowly expressed mRNAs (fig. S14). Second, computationally correcting for this bias by recalculating the contributions of mRNA, per-mRNA translation, and protein degradation rates while proportionally up-weighting the impact of underrepresented expression bins (29) does not affect our conclusions (fig. S15). Third, the correlation between our protein translation at baseline (t = 0 hours), as estimated with pulsed-SILAC data or TE values, is comparable when considering only the lowest expressed 25% (Pearson r ~ 0.52), the highest expressed 25% (r ~ 0.58), or all modeled proteins (r ~ 0.5) (fig. S16, A and B). Last, there is no significant difference in the distribution of TE values in the (underrepresented) lowly expressed mRNA bins between those proteins we detect (in the 3147 proteins) versus those we could not include in our model (P = 0.069, t test) (fig. S16C); thus, it is unlikely that the lowly expressed genes that we could not model have different regulatory modes.

Protein life-cycle changes primarily affect proteins performing basic cellular functions

Although mRNA fold changes contributed most to relative changes in protein expression (ratios of LPS to MOCK-simulated protein levels), protein synthesis and degradation rates do change significantly for 357 proteins (~11% of consistently detected proteins) (tables S7 and S8) (29) and in particular for proteins performing essential cellular functions ("housekeeping proteins") (Figs. 2B and 3E and table S6), including cytoskeletal, metabolic, ribosomal (Fig. 4A), and mitochondrial proteins (Fig. 4B). Because these are among the most abundant in the cell (13, 16, 37, 38), we reasoned that although mRNA changes may dominate the relative (fold) changes in protein levels after LPS stimulation, changes in the protein life cycle could contribute substantially more to differences in absolute cellular protein abundance than to relative changes. For example, consider two genes: Gene 1 is induced 10-fold from 10,000 to 100,000 proteins (a substantial change in relative protein abundance), whereas gene 2 is induced 1.2-fold from 1,000,000 to 1,200,000 proteins (a substantial change in absolute protein abundance). We asked whether relative and absolute changes are associated with different regulatory mechanisms. Indeed, we found that changes in translation and degradation rates together explain more of absolute protein changes than do changes in mRNA levels (mRNA, ~32 to 43% of the fit value; per-mRNA translation rates, ~22 to 41%; protein degradation rates, ~19 to 36%) (Fig. 3D and fig. S11C). Thus, posttranscriptional regulation contributes substantially more to absolute protein level changes than to relative protein level changes.

An increase in degradation rates of mitochondrial proteins is associated with mitophagy

Upon LPS stimulation, a substantial decrease in the level of mitochondrial proteins is associated with increased degradation rates, although these proteins are among the most stable in unstimulated DCs (Figs. 2B, 3E, and 4B and table S6). This increase in protein degradation is accompanied by a significant decrease ($P < 10^{-10}$, Wilcoxon rank sum test) (Fig. 3E and table S6) in mRNA levels and in per-mRNA translation rates ($P < 10^{-7}$, Wilcoxon rank sum test) (Fig. 3E and table S6), suggesting decreased production of new mitochondrial proteins and increased destruction of old ones. Both structural mitochondrial proteins and enzymes in key mitochondrial metabolic pathways have increased degradation. The increased degradation of key enzymes—such as Sucla2, Aldh2, and Aco2—is consistent with a

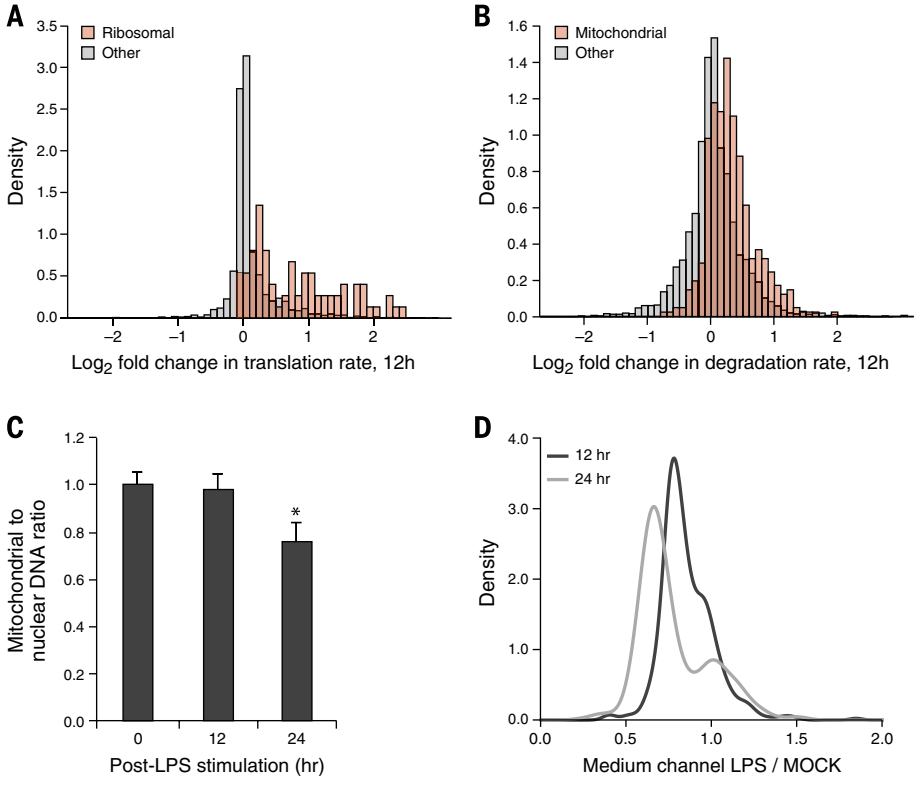

Fig. 4. Degradation of mitochondrial proteins after LPS stimulation is associated with mitophagy. (**A** and **B**) Increased translation rates of some ribosomal proteins (A) and increased degradation rates of mitochondrial proteins (B). Shown are the distributions of $\log_2$ fold changes of translation rates (ΔT_i, A) or degradation rates (ΔD_i, B) between LPS- and MOCK-stimulated cells of all measured ribosomal proteins [(A), red] or mitochondrial proteins [(B), red; from MitoCarta annotations (43)] and all measured proteins (gray). (**C**) Evidence of mitophagy in LPS-stimulated DCs. Shown is the mitochondrial to nuclear DNA ratio (y axis) in DCs at 0, 12, and 24 hours after LPS stimulation (x axis). Values are normalized to the average mitochondrial to nuclear DNA ratio at 0 hours. Asterisk indicates a significant change relative to 0 hours (P = 0.016, t test, n = 3 independent biological replicates). (**D**) Distribution of raw $\log_2$ LPS/MOCK M/L ratios (a proxy for protein decay) for all measured mitochondrial proteins [in MitoCarta (43)] at 12 hours (black) and 24 hours (gray) after stimulation.

reported shift in LPS-stimulated DCs from oxidative phosphorylation and oxygen consumption to glycolysis, glucose consumption, and lactate production (*39*–*42*).

The increased loss of structural proteins and enzymes in the mitochondria may be due to either a targeted metabolic shift in carbon and energy metabolism through a reduction of a specific subset of the mitochondrial proteome or a more global loss of entire mitochondria through mitophagy. To experimentally distinguish between the two hypotheses, we measured the mitochondrial-to-nuclear DNA ratio in unstimulated DCs and at 12 hours and 24 hours after LPS stimulation (the latter time point was chosen to account for any delay in complete mitochondrial DNA degradation) (Fig. 4C). There was no significant change in the ratio of mitochondrial-to-nuclear DNA at 12 hours after LPS stimulation, but there was a significant (~25%; $P = 0.016$, t test) reduction at 24 hours after stimulation (Fig. 4C). Indeed, analyzing pulsed SILAC data collected at 24 hours after LPS and mock stimulation, we saw a decrease in the M/L ratios (a proxy for increased degradation) of ~80% of annotated mitochondrial proteins in LPS versus MOCK samples (Fig. 4D) and in nearly all mitochondrial proteins with a higher mitochondrial localization prediction score [from MitoCarta (*43*)—over 95% of the 156 proteins with a score >20 of the 472 measured mitochondrial proteins] (fig. S17). These results suggest that mitophagy is a driver of LPS-induced mitochondrial protein degradation in DCs, which is consistent with previous observations of mitophagy in virus- or bacteria-infected DCs (*44*) and might also contribute to epitope presentation, as previously proposed (*45*).

Discussion

We determined the contribution of changes in mRNA levels, protein synthesis, and protein degradation rates during a dynamic response and found that changes in mRNA levels dominate relative fold changes. When considering also absolute changes in protein molecules (abundance), our data suggest a model in which the cellular proteome is dynamically regulated through two strategies.

In the first strategy, mRNA regulation acts primarily to ensure that specific functions—here, immune response proteins—are only expressed when needed and thus explains most of the fold-change differences in protein levels, contributing to LPS-induced protein fold changes at least 8 times as much as the combined protein life cycle within the 12-hour time scale of our measurements. It is possible that protein life-cycle changes are important to turn over key regulatory and signaling proteins at later phases of the response. Although our study does not directly address which steps in mRNA regulation account for this, our related work on the RNA life cycle during the first 3 hours in LPS-stimulated DCs suggests that transcriptional changes may in turn dominate differential mRNA expression, whereas dynamic changes in RNA processing or degradation affect only a minority of genes, albeit with important function (*46*). Furthermore, in contrast to previous reports in which degradation rates contributed only marginally (*16*, *20*), but consistent with Li *et al.* (*6*), we see that within the protein life cycle, changes in protein degradation rates play an equal role to changes in per-mRNA translation rates. Although some of this is due to turnover from increased secretion of some proteins (figs. S9C and S18), excluding the secretome (*33*) from our analysis did not strongly alter this global trend (fig. S18). Last, although mRNA changes dominate changes in protein levels, it may be difficult to discern this relationship in the absence of a model-driven analysis. Thus, whereas mRNA induction is readily reflected in protein level induction (fig. S19 and table S9), albeit somewhat dampened (fig. S19 and table S9), few of the 912 repressed mRNAs (more than twofold) show matching protein changes (fig. S19 and table S9). This could be naively interpreted as substantial posttranscriptional control, but preexisting proteins, the long protein half-life, and the delay of protein changes relative to mRNA changes (fig. S13) complicate such an intuitive interpretation, and our analysis shows that mRNA changes drive protein down-regulation as well (fig. S12 and table S5) (*29*).

In the second strategy, regulation at the protein level primarily readjusts the preexisting proteome, especially "housekeeping" proteins, in order to meet the requirements of a new cellular state, such as change in shape or metabolism. Thus, when we consider the contribution of a change in each rate to the change in the number of proteins (rather than the relative fold change), the contribution of changes in the protein life cycle is substantially increased (Fig. 3D). We find similar patterns of contributions when we use the Spearman rank correlation rather than Pearson correlation (fig. S20) (*29*), suggesting that our conclusions are robust to outliers with particularly strong changes.

The extent to which this two-part strategy applies in other dynamic settings remains to be determined. Recent studies comparing protein and translation rate differences between different states (for example, differentiated versus nondifferentiated cells or between different yeast strains) suggested that translation rate differences affect differential protein expression only modestly (*20*, *47*–*51*) but do affect some highly expressed proteins, including ribosomal proteins (*49*, *50*), which are also translationally regulated in our system.

Our analysis of unstimulated (resting) postmitotic DCs refines and extends previous models of protein level regulation in steady state. In our cells, nearly two thirds of the gene-to-gene variation in total protein levels is explained by regulation of mRNA levels—a higher contribution than previously reported in dividing mammalian cells (*16*), possibly because of the regulatory mechanisms active in primary postmitotic, homeostatic resting cells. For example, the increased role we observed for protein degradation, in contrast to prior studies (*16*, *20*), may be needed by postmitotic cells that cannot simply renew their protein pool through division-coupled passive dilution. Furthermore, our analysis corrected for RNA-Seq expression reproducibility, intralibrary protein expression reproducibility, and library-dependent protein expression biases (fig. S21) (*29*), all of which are essential to avoid inadvertent attribution of measurement errors to modeled translation and protein degradation rates. Indeed, whereas from raw data mRNA explains 27% of the gene-to-gene variation in protein levels at baseline ($t = 0$), using modeled expression values it explains 42%, and once correcting for data reproducibility (*29*), it explains 52%. This compares well with a recent study (*6*) that found that mRNA levels explain at least 56% of the differences in protein abundance [when estimating the variances of errors with control measurements (*16*)] and possibly as much as ~84% [using TE values to estimate the systematic error in translation rates in (*16*)]. Each of these strategies highlights the importance of determining and correcting for stochastic and systematic errors in the data. Even with our conservative estimates, the protein life cycle is estimated to contribute, at minimum, about a third of the final steady-state protein expression level. Because protein expression levels span around 4 to 5 orders of magnitude (*13*, *16*, *37*, *38*), differences between genes in the protein life cycle can easily cause a 10- to 100-fold change in protein expression.

Our experimental and analytical design should be broadly applicable to study similar events in diverse dynamical cell systems. Our analytical model distinguishes per-mRNA translation and protein degradation rates that were confounded in previous, model-free analyses of raw H/L and M/L ratios from dynamic pulsed-SILAC data (*20*) because of, for example, the contribution of mRNA and protein degradation to the H/L signal and of recycled labeled amino acids to the M/L signal (*29*). Our empirical Bayes strategy also handles noise in proteomics data in a principled and conservative way. Nevertheless, we make some simplifying assumptions in our model (such as linear changes in per-mRNA translation rates and degradation rates) that may be refined in the future [for example, with sigmoidal functions (*22*, *52*, *53*)], allowing us to estimate additional valuable parameters (such as time point of rate change). This would require finer-resolution data, such as from ribosome profiling (*49*, *54*, *55*), puromycin-associated nascent chain proteomics (*56*), or the combination of pulsed-SILAC labeling with pulse-labeling by using the methionine analog azidohomoalanine (*33*, *57*). Such enhanced methods will provide a framework to study the contributions of the protein life cycle in diverse dynamic systems and help identify new key regulators of these responses.

REFERENCES AND NOTES

1. N. Sonenberg, A. G. Hinnebusch, Regulation of translation initiation in eukaryotes: Mechanisms and biological targets. *Cell* **136**, 731–745 (2009). doi: 10.1016/j.cell.2009.01.042; pmid: 19239892
2. M. A. Chapman *et al.*, Initial genome sequencing and analysis of multiple myeloma. *Nature* **471**, 467–472 (2011). doi: 10.1038/nature09837; pmid: 21430775

3. A. Castello, B. Fischer, M. W. Hentze, T. Preiss, RNA-binding proteins in Mendelian disease. *Trends Genet.* **29**, 318–327 (2013). doi: 10.1016/j.tig.2013.01.004; pmid: 23415593
4. S. Komili, P. A. Silver, Coupling and coordination in gene expression processes: A systems biology view. *Nat. Rev. Genet.* **9**, 38–48 (2008). doi: 10.1038/nrg2223; pmid: 18071322
5. C. Vogel, E. M. Marcotte, Insights into the regulation of protein abundance from proteomic and transcriptomic analyses. *Nat. Rev. Genet.* **13**, 227–232 (2012). pmid: 22411467
6. J. J. Li, P. J. Bickel, M. D. Biggin, System wide analyses have underestimated protein abundances and the importance of transcription in mammals. *PeerJ.* **2**, e270 (2014). doi: 10.7717/peerj.270; pmid: 24688849
7. S. P. Gygi, Y. Rochon, B. R. Franza, R. Aebersold, Correlation between protein and mRNA abundance in yeast. *Mol. Cell. Biol.* **19**, 1720–1730 (1999). pmid: 10022859
8. R. de Sousa Abreu, L. O. Penalva, E. M. Marcotte, C. Vogel, Global signatures of protein and mRNA expression levels. *Mol. Biosyst.* **5**, 1512–1526 (2009). pmid: 20023718
9. T. Maier, M. Güell, L. Serrano, Correlation of mRNA and protein in complex biological samples. *FEBS Lett.* **583**, 3966–3973 (2009). doi: 10.1016/j.febslet.2009.10.036; pmid: 19850042
10. C. Vogel *et al.*, Sequence signatures and mRNA concentration can explain two-thirds of protein abundance variation in a human cell line. *Mol. Syst. Biol.* **6**, 400 (2010). doi: 10.1038/msb.2010.59; pmid: 20739923
11. S. P. Schrimpf *et al.*, Comparative functional analysis of the *Caenorhabditis elegans* and *Drosophila melanogaster* proteomes. *PLOS Biol.* **7**, e48 (2009). doi: 10.1371/journal.pbio.1000048; pmid: 19260763
12. S. Marguerat *et al.*, Quantitative analysis of fission yeast transcriptomes and proteomes in proliferating and quiescent cells. *Cell* **151**, 671–683 (2012). doi: 10.1016/j.cell.2012.09.019; pmid: 23101633
13. M. Wilhelm *et al.*, Mass-spectrometry-based draft of the human proteome. *Nature* **509**, 582–587 (2014). doi: 10.1038/nature13319; pmid: 24870543
14. M. Weiss, S. Schrimpf, M. O. Hengartner, M. J. Lercher, C. von Mering, Shotgun proteomics data from multiple organisms reveals remarkable quantitative conservation of the eukaryotic core proteome. *Proteomics* **10**, 1297–1306 (2010). doi: 10.1002/pmic.200900414; pmid: 20077411
15. Z. Khan *et al.*, Primate transcript and protein expression levels evolve under compensatory selection pressures. *Science* **342**, 1100–1104 (2013). doi: 10.1126/science.1242379; pmid: 24136357
16. B. Schwanhäusser *et al.*, Global quantification of mammalian gene expression control. *Nature* **473**, 337–342 (2011). doi: 10.1038/nature10098; pmid: 21593866
17. C. Vogel, G. M. Silva, E. M. Marcotte, Protein expression regulation under oxidative stress. *Mol. Cell. Proteomics* **10**, 009217 (2011). doi: 10.1074/mcp.M111.009217; pmid: 21933953
18. M. V. Lee *et al.*, A dynamic model of proteome changes reveals new roles for transcript alteration in yeast. *Mol. Syst. Biol.* **7**, 514 (2011). doi: 10.1038/msb.2011.48; pmid: 21772262
19. T. Maier *et al.*, Quantification of mRNA and protein and integration with protein turnover in a bacterium. *Mol. Syst. Biol.* **7**, 511 (2011). doi: 10.1038/msb.2011.38; pmid: 21772259
20. A. R. Kristensen, J. Gsponer, L. J. Foster, Protein synthesis rate is the predominant regulator of protein expression during differentiation. *Mol. Syst. Biol.* **9**, 689 (2013). doi: 10.1038/msb.2013.47; pmid: 24045637
21. R. M. Steinman, J. Banchereau, Taking dendritic cells into medicine. *Nature* **449**, 419–426 (2007). doi: 10.1038/nature06175; pmid: 17898760
22. M. Rabani *et al.*, Metabolic labeling of RNA uncovers principles of RNA production and degradation dynamics in mammalian cells. *Nat. Biotechnol.* **29**, 436–442 (2011). doi: 10.1038/nbt.1861; pmid: 21516085
23. I. Mellman, R. M. Steinman, Dendritic cells: Specialized and regulated antigen processing machines. *Cell* **106**, 255–258 (2001). doi: 10.1016/S0092-8674(01)00449-4; pmid: 11509172
24. I. Amit *et al.*, Unbiased reconstruction of a mammalian transcriptional network mediating pathogen responses. *Science* **326**, 257–263 (2009). doi: 10.1126/science.1179050; pmid: 19729616
25. M. Garber *et al.*, A high-throughput chromatin immunoprecipitation approach reveals principles of dynamic gene regulation in mammals. *Mol. Cell* **47**, 810–822 (2012). doi: 10.1016/j.molcel.2012.07.030; pmid: 22940246
26. N. Chevrier *et al.*, Systematic discovery of TLR signaling components delineates viral-sensing circuits. *Cell* **147**, 853–867 (2011). doi: 10.1016/j.cell.2011.10.022; pmid: 22078882
27. A. K. Shalek *et al.*, Single-cell transcriptomics reveals bimodality in expression and splicing in immune cells. *Nature* **498**, 236–240 (2013). doi: 10.1038/nature12172; pmid: 23685454
28. F.-M. Boisvert *et al.*, A quantitative spatial proteomics analysis of proteome turnover in human cells. *Mol. Cell. Proteomics* **11**, 011429 (2012). doi: 10.1074/mcp.M111.011429; pmid: 21937730
29. Materials and methods are available as supplementary materials on *Science* Online.
30. A. O. Subtelny, S. W. Eichhorn, G. R. Chen, H. Sive, D. P. Bartel, Poly(A)-tail profiling reveals an embryonic switch in translational control. *Nature* **508**, 66–71 (2014). doi: 10.1038/nature13007; pmid: 24476825
31. E. K. Schmidt, G. Clavarino, M. Ceppi, P. Pierre, SUnSET, a nonradioactive method to monitor protein synthesis. *Nat. Methods* **6**, 275–277 (2009). doi: 10.1038/nmeth.1314; pmid: 19305406
32. H. Lelouard *et al.*, Regulation of translation is required for dendritic cell function and survival during activation. *J. Cell Biol.* **179**, 1427–1439 (2007). pmid: 18166652
33. K. Eichelbaum, M. Winter, M. Berriel Diaz, S. Herzig, J. Krijgsveld, Selective enrichment of newly synthesized proteins for quantitative secretome analysis. *Nat. Biotechnol.* **30**, 984–990 (2012). doi: 10.1038/nbt.2356; pmid: 23000932
34. T. Sanada *et al.*, FLN29 deficiency reveals its negative regulatory role in the Toll-like receptor (TLR) and retinoic acid-inducible gene I (RIG-I)-like helicase signaling pathway. *J. Biol. Chem.* **283**, 33858–33864 (2008). doi: 10.1074/jbc.M806923200; pmid: 18849341
35. A. P. Kuan *et al.*, Genetic control of autoimmune myocarditis mediated by myosin-specific antibodies. *Immunogenetics* **49**, 79–85 (1999). doi: 10.1007/s002510050466; pmid: 9887344
36. P. R. Burton *et al.*, Genome-wide association study of 14,000 cases of seven common diseases and 3,000 shared controls. *Nature* **447**, 661–678 (2007). doi: 10.1038/nature05911; pmid: 17554300
37. M.-S. Kim *et al.*, A draft map of the human proteome. *Nature* **509**, 575–581 (2014). doi: 10.1038/nature13302; pmid: 24870542
38. T. Geiger *et al.*, Initial quantitative proteomic map of 28 mouse tissues using the SILAC mouse. *Mol. Cell. Proteomics* **12**, 1709–1722 (2013). doi: 10.1074/mcp.M112.024919; pmid: 23436904
39. B. Everts *et al.*, Commitment to glycolysis sustains survival of NO-producing inflammatory dendritic cells. *Blood* **120**, 1422–1431 (2012). doi: 10.1182/blood-2012-03-419747; pmid: 22786879
40. C. M. Krawczyk *et al.*, Toll-like receptor-induced changes in glycolytic metabolism regulate dendritic cell activation. *Blood* **115**, 4742–4749 (2010). doi: 10.1182/blood-2009-10-249540; pmid: 20351312
41. E. L. Pearce, E. J. Pearce, Metabolic pathways in immune cell activation and quiescence. *Immunity* **38**, 633–643 (2013). doi: 10.1016/j.immuni.2013.04.005; pmid: 23601682
42. B. Everts *et al.*, TLR-driven early glycolytic reprogramming via the kinases TBK1-IKKε supports the anabolic demands of dendritic cell activation. *Nat. Immunol.* **15**, 323–332 (2014). doi: 10.1038/ni.2833; pmid: 24562310
43. D. J. Pagliarini *et al.*, A mitochondrial protein compendium elucidates complex I disease biology. *Cell* **134**, 112–123 (2008). doi: 10.1016/j.cell.2008.06.016; pmid: 18614015
44. C. Lupfer *et al.*, Receptor interacting protein kinase 2-mediated mitophagy regulates inflammasome activation during virus infection. *Nat. Immunol.* **14**, 480–488 (2013). doi: 10.1038/ni.2563; pmid: 23525089
45. C. Bell *et al.*, Quantitative proteomics reveals the induction of mitophagy in TNF-α activated macrophages. *Mol. Cell. Proteomics* **12**, 2394–2407 (2013). doi: 10.1074/mcp.M112.025775
46. M. Rabani *et al.*, High-resolution sequencing and modeling identifies distinct dynamic RNA regulatory strategies. *Cell* **159**, 1698–1710 (2014). doi: 10.1016/j.cell.2014.11.015; pmid: 25497548
47. D. Baek *et al.*, The impact of microRNAs on protein output. *Nature* **455**, 64–71 (2008). doi: 10.1038/nature07242; pmid: 18668037
48. M. Selbach *et al.*, Widespread changes in protein synthesis induced by microRNAs. *Nature* **455**, 58–63 (2008). doi: 10.1038/nature07228; pmid: 18668040
49. N. T. Ingolia, L. F. Lareau, J. S. Weissman, Ribosome profiling of mouse embryonic stem cells reveals the complexity and dynamics of mammalian proteomes. *Cell* **147**, 789–802 (2011). doi: 10.1016/j.cell.2011.10.002; pmid: 22056041
50. A. C. Hsieh *et al.*, The translational landscape of mTOR signalling steers cancer initiation and metastasis. *Nature* **485**, 55–61 (2012). doi: 10.1038/nature10912; pmid: 22367541
51. F. W. Albert, D. Muzzey, J. S. Weissman, L. Kruglyak, Genetic influences on translation in yeast. *PLOS Genet.* **10**, e1004692 (2014). doi: 10.1371/journal.pgen.1004692; pmid: 25340754
52. G. Chechik *et al.*, Activity motifs reveal principles of timing in transcriptional control of the yeast metabolic network. *Nat. Biotechnol.* **26**, 1251–1259 (2008). doi: 10.1038/nbt.1499; pmid: 18953355
53. N. Yosef, A. Regev, Impulse control: Temporal dynamics in gene transcription. *Cell* **144**, 886–896 (2011). doi: 10.1016/j.cell.2011.02.015; pmid: 21414481
54. N. T. Ingolia, S. Ghaemmaghami, J. R. S. Newman, J. S. Weissman, Genome-wide analysis in vivo of translation with nucleotide resolution using ribosome profiling. *Science* **324**, 218–223 (2009). doi: 10.1126/science.1168978; pmid: 19213877
55. N. Stern-Ginossar *et al.*, Decoding human cytomegalovirus. *Science* **338**, 1088–1093 (2012). doi: 10.1126/science.1227919; pmid: 23180859
56. R. Aviner, T. Geiger, O. Elroy-Stein, Novel proteomic approach (PUNCH-P) reveals cell cycle-specific fluctuations in mRNA translation. *Genes Dev.* **27**, 1834–1844 (2013). doi: 10.1101/gad.219105.113; pmid: 23934657
57. K. Eichelbaum, J. Krijgsveld, Rapid temporal dynamics of transcription, protein synthesis, and secretion during macrophage activation. *Mol. Cell. Proteomics* **13**, 792–810 (2014). doi: 10.1074/mcp.M113.030916; pmid: 24396086

ACKNOWLEDGMENTS

We thank members of the Regev, Hacohen, and Carr groups, as well as G. Brar, N. Slavov, and E. Airoldi for constant input and discussions. We thank L. Gaffney for help with the figures and K. Lage and A. Kashani for help with some of the analyses. This work was supported by National Human Genome Research Institute Centers of Excellence in Genomics Science P50 HG006193 (A.R, N.H., S.A.C.) and Broad Institute Funds. A.R. was supported by an NIH Pioneer Award, the Klarman Cell Observatory, and HHMI. M.J. was supported by fellowships of the Swiss National Science Foundation for advanced researchers (SNF) and the Marie Sklodowska-Curie International Outgoing Fellowships. M.S.R. was supported by the NIH Training Program in Bioinformatics and Integrative Genomics training grant. S.S. was supported by a Rothschild Fellowship, a European Molecular Biology Organization fellowship, and Human Frontier Science Program fellowships. E.H.R. was supported by the Howard Hughes Medical Institute Gilliam Fellowship for Advanced Study. Data have been deposited in the Gene Expression Omnibus under accession number GSE59793. The original mass spectra may be downloaded from MassIVE (http://massive.ucsd.edu) using the identifier MSV000078994. The data are accessible at ftp://MSV000078994:a@massive.ucsd.edu. DogmaQuant is distributed under open source (BSD) license.

SUPPLEMENTARY MATERIALS

www.sciencemag.org/content/347/6226/1259038/suppl/DC1
Materials and Methods
Figs. S1 to S21
R Script for Estimation of Translation and Degradation Rates (Baseline and Fold Change)
References (*58*–*73*)
Tables S1 to S9

22 July 2014; accepted 23 January 2015
Published online 12 February 2015;
10.1126/science.1259038

Dynamic profiling of the protein life cycle in response to pathogens

Marko Jovanovic, Michael S. Rooney, Philipp Mertins, Dariusz Przybylski, Nicolas Chevrier, Rahul Satija, Edwin H. Rodriguez, Alexander P. Fields, Schraga Schwartz, Raktima Raychowdhury, Maxwell R. Mumbach, Thomas Eisenhaure, Michal Rabani, Dave Gennert, Diana Lu, Toni Delorey, Jonathan S. Weissman, Steven A. Carr, Nir Hacohen and Aviv Regev

Science **347** (6226), 1259038.
DOI: 10.1126/science.1259038originally published online February 12, 2015

How the immune system readies for battle

Although gene expression is tightly controlled at both the RNA and protein levels, the quantitative contribution of each step, especially during dynamic responses, remains largely unknown. Indeed, there has been much debate whether changes in RNA level contribute substantially to protein-level regulation. Jovanovic *et al.* built a genome-scale model of the temporal dynamics of differential protein expression during the stimulation of immunological dendritic cells (see the Perspective by Li and Biggin). Newly stimulated functions involved the up-regulation of specific RNAs and concomitant increases in the levels of the proteins they encode, whereas housekeeping functions were regulated posttranscriptionally at the protein level.

Science, this issue 10.1126/science.1259038; see also p. 1066